Acta Pharmaceutica Sinica B 2018;8(3):360–370

Chinese Pharmaceutical Association
Institute of Materia Medica, Chinese Academy of Medical Sciences

Acta Pharmaceutica Sinica B

www.elsevier.com/locate/apsb
www.sciencedirect.com

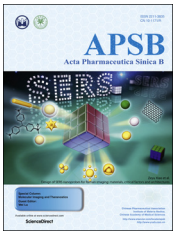

REVIEW

Radiopaque nano and polymeric materials for atherosclerosis imaging, embolization and other catheterization procedures

Li Tian[a], Linfeng Lu[a], James Feng[b], Marites P. Melancon[a,c,*]

[a]*Department of Interventional Radiology, The University of Texas MD Anderson Cancer Center, Houston, TX 77030, USA*
[b]*Duke University, Durham, NC 27708, USA*
[c]*Graduate School of Biomedical Sciences, University of Texas Health Science Center at Houston, Houston, TX 77030, USA*

Received 3 November 2017; received in revised form 18 January 2018; accepted 8 February 2018

KEY WORDS

Radiopaque contrast nanoparticles and materials;
X-ray;
CT;
Vascular diseases;
Atherosclerosis;
Plaque;
Stenosis;
Embolization;
Inferior vena cava filters

Abstract A review of radiopaque nano and polymeric materials for atherosclerosis imaging and catheterization procedures is presented in this paper. Cardiovascular diseases (CVDs) are the leading cause of death in the US with atherosclerosis as a significant contributor for mortality and morbidity. In this review paper, we discussed the physics of radiopacity and X-ray/CT, clinically used contrast agents, and the recent progress in the development of radiopaque imaging agents and devices for the diagnosis and treatment of CVDs. We focused on radiopaque imaging agents for atherosclerosis, radiopaque embolic agents and drug eluting beads, and other radiopaque medical devices related to catheterization procedures to treat CVDs. Common strategies of introducing radiopacity in the polymers, together with examples of their applications in imaging and medical devices, are also presented.

*Corresponding author at: Department of Interventional Radiology, The University of Texas MD Anderson Cancer Center, Houston, TX 77030, USA.
E-mail address: mmelancon@mdanderson.org (Marites P. Melancon).

Peer review under responsibility of Institute of Materia Medica, Chinese Academy of Medical Sciences and Chinese Pharmaceutical Association.

https://doi.org/10.1016/j.apsb.2018.03.002

1. Introduction

Cardiovascular disease (CVD) is responsible for a significant percentage of morbidity, mortality, and financial burden on individuals and families, particularly in developed countries like the United States[1]. Common manifestations of these diseases include vascular stenosis such as atherosclerosis, hypertension, chronic obstructive pulmonary disease, and blood-clotting disorders such as embolisms and thromboses. Though cardiovascular and blood diseases can be attributed to a variety of factors, the aging of the general population has been correlated with an increasingly prevalent diagnosis in medical practice[2,3]. The 2017 Heart Disease and Stroke Statistics Update compiled by the American Heart Association revealed that nearly 801,000 deaths were attributed to CVD, making it the leading cause of death in the United States and claiming more lives than all forms of cancer and lower respiratory diseases combined[4]. Four hundred ninety six thousand, or 61.5% of these deaths were attributed to vascular stenosis-related diseases or complications[4]. In 2010, an estimated 7,588,000 inpatient cardiovascular operations and procedures were performed in the United States and CVD also ranked highest in the number of hospital patient discharges. It should be noted that these figures only represent clinical data. It is estimated that 92.1 million US adults live with some degree of CVD. Of these, 46.7 million are estimated to be 60 years of age or older and a total of 11.5% of American adults (27.6 million) have been diagnosed with heart disease. By 2030, 43.9% of the US adult population is projected to have some form of CVD[4].

2. Radiopacity and the application in CVD imaging

Embolization procedures are often guided by ultrasound and X-ray imaging. Ultrasound is a non-invasive imaging modality which uses sound waves that have frequencies higher than what human can hear. A sound wave is generated by a transducer and partially reflected when there is a change in the acoustic impedance. The ultrasound collects the reflected waves, or echoes, and transforms them into digital images. Intravascular ultrasound has been used extensively for cardiovascular imaging and catheterization procedures[5,6]. Compared to ultrasound, X-rays have even higher frequencies, and can provide more detailed and clear images. X-ray fluoroscopy shows real-time images, facilitating interventional procedures like the guidance of catheters for embolization, and an X-ray angiogram can be used to map the vasculature along with any abnormalities like stenosis or thrombosis[7,8]. More recently, computed tomography (CT) has also been used as a noninvasive alternative to traditional X-ray techniques[9] to produce three-dimensional images and show size, shape, and composition[10,11]. However, X-ray is limited in the contrast it can provide toward differentiating between different soft tissue and healthy and pathological tissue[7]. Therefore, a contrast agent with a different radiopacity than the surrounding tissues is often used to enhance the images. We will introduce the basics of radiopacity in the following paragraphs.

2.1. Physics of X-ray and radiopacity

Although there are many different applications of X-rays, the physics behind the phenomena is largely the same. X-rays are produced by the collision and deflection of accelerated electrons with the target. The two types of resultant radiation are called Bremsstrahlung and characteristic radiation. The deflected incident electrons continue producing Bremsstrahlung and characteristic radiation until its energy is depleted[11].

In the diagnostic energy ranges, the photoelectric effect, the main form of interaction between X-ray photons and the subjects, and the Compton effect are the two processes through which photons can interact with the absorbing subject. Fig. 1 shows the relative amount of interactions by the photoelectric effect and the Compton effect[12]. The photoelectric effect occurs when a X-ray photon of higher energy than the k-/l-edge energy of the target transfers all of its energy to an inter-shell electron, causing the photon to cease to exist while a photoelectron is emitted[11,13]. The atom will then emit characteristic X-rays when a higher energy electron fills in the void left by the photoelectron.

For a CT contrast agent to be effective, images need to be taken with peak voltages higher than the k-edge of the agent, providing contrast enhancement between the surroundings and the agent itself. Hounsfield units $(HU)=1000\times(\mu-\mu_{water})/(\mu_{water}-\mu_{air})$ quantify X-ray attenuation, where μ are linear attenuation coefficients. The Hounsfield scale is standardized based on $HU_{water}=0$ and $HU_{air}=-1000$[13,14].

2.2. Clinically used radiopaque contrast agents

For vasculature and tissues to be differentiated by visual inspection, radiopaque contrast agents are administered to the areas of interest, which increases the attenuation of the targeted tissues. CT contrast agents are usually elements with large atomic numbers like iodine, barium, gold, or bismuth that have k-/l-edges of higher energies than tissue to facilitate the absorption of X-ray photons[13,15]. For CT, iodinated contrast agents are the most prevalent and FDA approved.

Iodinated contrast agents are commonly used intravenously to visualize organs and vasculature[13]. However, iodinated contrast agents also are rapidly cleared by the kidney, which means that higher doses must be given for longer CT scans[13,16]. Side effects of the iodinated agents can include contrast-induced nephropathy, nausea, vomiting, and even anaphylaxis[17,18]. Furthermore, CT contrast agents are usually on the molar concentration scale, which has researchers looking for new contrast agents with greater imaging capabilities, smaller dose requirements, and lower toxicity[14].

Small molecule iodinated contrast agents can be ionic and nonionic. Compared with nonionic contrast agents, ionic contrast agents have greater chances to interact with biological structures and have high osmolality, possibly resulting in issues like osmotic dilution and renal toxicity[19–21]. The structure of these contrast agents usually contains single or double aromatic rings[14]. Fig. 2 shows the structure of iohexol (Omnipaque), a single aromatic ring molecule. Some commercially available small molecule iodinated contrast agents are listed in Table 1.

While lanthanide-based contrast agents, specifically gadolinium chelates, are used in MRI imaging, they can also act as CT contrast agents in cardiovascular and pulmonary angiographies because of high atomic numbers, leading to better attenuation[14,22]. Gadoxetate disodium, brand name Eovist, made by Bayer Healthcare, is a contrast agent that can be used for CT imaging the liver[14,23]. However, although gadolinium compounds can be used as both MRI and CT contrast agents due to its chemical and physical properties, more research is needed to improve their efficacy as multimodal contrast agents[14]. Multimodal contrast agents based on

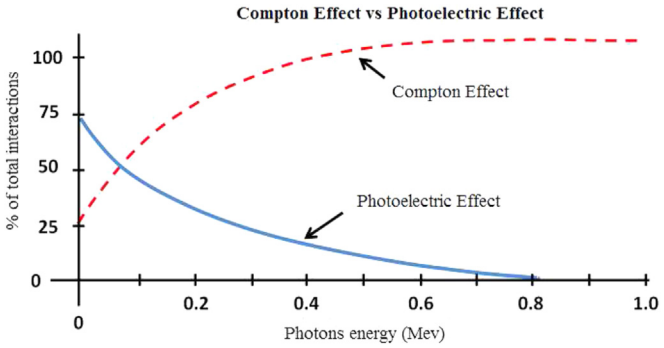

Figure 1 At most diagnostic CT energy levels, the photoelectric effect is dominant. Image taken from Ref. 12. Available from: ⟨https://www.intechopen.com/books/advanced-image-acquisition-processing-techniques-and-applications-i/high-density-devices-applied-to-a-gamma-camera-implementation⟩, which is licensed under CC BY 3.0.

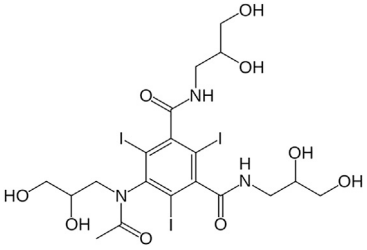

Figure 2 Molecular structure of iohexol (Omnipaque), a small molecule iodinated single aromatic ring contrast agent available for commercial use.

Table 1 Commercially available small-molecule iodinated contrast agents.

Category	Generic name	Brand name	Manufacturer
Ionic	Diatrizoate	Gastrografin	Therapex
	Iothalamate	Conray	Liebel-Flarsheim Company
Nonionic	Iodixanol	Visipaque	GE Healthcare
	Iohexol	Omnipaque	GE Healthcare
	Iopamidol	Isovue	BIPSO GmbH
	Iopromide	Ultravist	Bayer Healthcare
	Ioversol	Optiray	Liebel-Flarsheim Company
	Ioxilan	Oxilan	Guerbet LLC

perfluorooctyl bromide have been used for many years to help image the liver, spleen, and vasculature[13,24]. Barium sulfate is a common orally-taken contrast agent used for imaging of the gastrointestinal tract[25]. In some countries, xenon gas is used clinically as an alternative to iodinated media in cerebrovascular imaging[26]. Xenon has a short half-life of around 30 s; side effects related to its anesthetic properties include nausea, headaches, and vomiting[27].

3. Radiopaque nanoparticles and biomaterials for atherosclerosis imaging and catheterization procedures

Vascular stenosis is the most prevalent and leading cause of death in those affected by CVD[28]. Healthy arteries are flexible and have smooth inner walls free from occlusion and pressure. However, vascular stenosis occurs when a progressive narrowing of the lumen obstructs local blood flow and inhibits the perfusion of tissue and organs. Vascular stenosis can manifest from extrinsic or intrinsic conditions. Extrinsic stenosis is caused by external compression on arteries usually as the result of tumors, aneurysms or foreign objects, which obstructs optimal blood flow[29]. Intrinsic stenosis, or atherosclerosis, is a condition of intramural buildup and interaction of high concentrations of apolipoprotein B-containing lipoproteins, cells such as macrophages, dendritic cells, T cells, and other cellular material inside medium to large thick-walled arteries. This volatile interaction leads to an inflammatory response and eventually the development of complex lesions, or plaques, that extend into and narrow the arterial lumen[30]. These plaque lesions can rupture and thrombosis can migrate, preventing the flow of oxygen rich blood to vital tissue and organs including the heart (coronary artery disease), brain (ischemic stroke) or the lower extremities (peripheral vascular disease)[31]. An increased blood concentration of apolipoprotein B–containing lipoproteins, can be enough to cause atherosclerosis, such as in familial hypercholesterolemia[32]. In most cases, however, atherosclerosis is able to develop at lower concentrations in combination with other potential risk factors including hypertension, smoking, obesity, male sex, and genetic susceptibility to the disease[32,33], which suggests the multifactorial nature of the disease. The most serious vascular stenosis disease is congenital heart disease (CHD), which often leads to the clinical complications of myocardial infarction and angina pectoris, and cerebrovascular disease, which often leads to stroke[34]. Myocardial infarction and stroke were the two highest causes of death in those affected by cardiovascular disease in 2016, accounting for 45.1% and 16.5% of death respectively[4]. Due to the prevalence of vascular stenosis morbidity and mortality, a consistently successful treatment of atherosclerosis has been a highly desirable clinical achievement.

Current standard treatment varies by severity and risk of the disease but includes diet and lifestyle changes[35], lipid reduction medications such as MG-CoA reductase inhibitors[36], and therapeutic agents targeting various factors[37], such as chemokine[38–40] and corresponding receptors[41,42], macrophage migration inhibitory factor[43,44], platelets[45–48], and so on. In severe cases, surgical treatments include highly invasive interventions such as coronary artery bypass grafting[49] that uses autologous vessels to bypass diseased coronary arteries, carotid endarterectomy[50] that removes plaque buildup, and percutaneous coronary intervention[51] that opens up blocked or narrowed coronary arteries. In a percutaneous coronary intervention

procedure, under the image guidance of X-ray fluoroscopy, an interventional radiologist or a cardiologist inserts a catheter into the diseased coronary artery from the femoral artery and uses a balloon from the catheter tip to open narrowed arteries. Sometimes, a stent is also deployed during the procedure to ensure blood flow through the diseased vessels[51].

Aside from opening up occluded blood vessels *via* balloon catheter and stent, the catheterization technique can also be used to deliver medication or artificial embolic agents to block blood flow to an area of the body, termed embolization. An embolization procedure is usually image guided by ultrasound or X-ray. When X-ray fluoroscopy is used, the embolic agents are usually mixed with a contrast agent, and the mixture is injected *via* the catheter. The X-ray fluoroscopy monitors the injection and the flow of the mixture in real time, and the catheter guides the delivery of the embolic agents to the vessels of interest[52]. X-ray fluoroscopy has many applications that are extraordinarily diverse. As a pathological procedure, it is used extensively in occluding internal hemorrhages such as gastrointestinal bleeding, cerebral aneurysms, postpartum bleeding and surgical/traumatic bleeding[53]. A significant emerging application of embolization is its potential as a treatment for certain types of cancer. In tumor therapy, embolization is used to reduce tumors by slowing or stopping blood supply to cancerous cells[54,55]. Embolic agents in the form of liquid and small particles are manipulated to create capillary occlusion, though it should be noted that this can lead to higher risk of necrosis and ischemia[53]. The occlusion is commonly built through an endovascular procedure but the result can also be achieved by other means such as by percutaneous injection of embolic agents into the tumor[56]. In cancer treatment applications, the embolic agents, in addition to blocking blood supply to the tumor, can also be used as a mechanism for delivering drugs to attack the tumor chemically[57]. However, most commercially available embolic agents are radiolucent. To make them radiopaque, embolic agents are mixed with iodine-based contrast agents. However, once the contrast agent has circulated off, it is difficult to determine the location and integrity of these embolic agents. Thus, researches have been focused on the development of radiopaque embolic agents that could be easily monitored by X-ray without the help of external mixing of contrast agents.

The development of radiopaque nanomaterials is aimed at improving the shortcomings of the above-mentioned small molecular weight contrast agents, such as oxicity and short imaging window. The general goal of its development is to enhance the contrast of either the diseased area or the nanomaterials themselves for easy deployment and long-term monitoring. In this review, we surveyed from published literature the various nanoparticles and biomaterials used for imaging atherosclerosis and catheterization procedures.

3.1. Research and development of nanoparticle contrast agents for atherosclerosis imaging

From the abovementioned discussion, the toxicity mainly comes from the contact between iodine and the blood or tissue components, and the short imaging window is from the fast clearance of small molecular weight iodine. Thus, research and development of radiopaque nanomaterials is focused on masking iodine in the nanomaterials by physical entrapment, chemical conjugation or polymerization, thus preventing the contact of bare iodine molecule, confining the radiopacity to the polymeric chain and prolonging the half-life of the polymerized iodine. Alternatively, noble elements with higher Z numbers are also synthesized into nanoparticles as contrast agents. These noble elements are toxic in their ionic forms, but as nanoparticles are either inert or made biocompatible by surface modification. The nanoparticle structures include nanoemulsion, micelle, dendrimer, and liposome. Nanoemulsion, for instance, has also been used in small molecular weight contrast agent, such as Lipiodol, an iodinated contrast agent made from poppy-seed oil[58,59]. Compared with small molecular weight contrast agents, these nanoparticles usually have less toxicity and longer circulation in the body. More importantly, the nanoparticles can undergo surface modification to target specific lesions for more accurate imaging.

While the calcification of atherosclerotic plaque provides a good CT imaging of the target, the progression of atherosclerosis also offers other targets including macrophages and fibrin[60]. Macrophages can uptake large amounts of nanomaterials and contribute to the poor delivery efficiency. However, macrophages also accumulate in the plaque and offer a good target for CT imaging. For example, Hyafil et al.[61] developed a suspension containing crystalline iodinated particles, N1177, for noninvasive macrophage imaging (Fig. 3). N1177 did not affect the viability of J774 macrophages or their phagocytic capacity or cytokine production[62]. Two hours after injection, N1177 accumulated in the macrophages in the atherosclerotic plagues on a rabbit model (Fig. 4)[63]. Another study done by Cormode et al.[64] used gold high-density lipoprotein nanoparticle contrast agent (Au-HDL) and a multicolor CT to characterize the macrophage burden, calcification, and stenosis of atherosclerotic plaques. Au-HDL mainly localized in the macrophages, and the multicolor CT was able to differentiate Au-HDL, iodine based contrast agent, and calcified material in the atherosclerosis.

Similar to macrophages, fibrin is also accumulated in atherosclerotic plaque and a good target for atherosclerosis imaging. The fibrin monomers are generated by cleavage of fibrinogen, which then polymerize and crosslink to form a stable clot. Fibrin deposition can initiate and contribute to plaque growth, and thrombus formation on ruptured atherosclerotic plaques is a precursor of myocardial infarction and stroke[65]. Thus, fibrin targeted imaging could reveal information not only on the plaque but also identify "vulnerable" plaques that may lead to myocardial infarction and stroke. Winter et al.[66] conjugated anti-fibrin F(ab)' fragments to iodinated oil nanoparticle and imaged such "vulnerable" human fibrin clots *in vitro*.

3.2. Recent progress on the development of radiopaque polymeric materials for medical devices or agents for embolization and other catheterization procedures

The application of nanoparticle contrast agents and the development of radiopaque polymeric materials are to improve existing treatment or devices. Current existing vascular implants or medical devices are usually made of various metals with an inert surface. They are highly radiopaque, but other properties are suboptimal, such as the inability of inert surfaces to seal aneurysms or the non-degradability that requires surgical removal after the intended use. Radiopaque polymeric materials are versatile and aimed at improving these shortcomings when forged into these medical devices. In this section, we will briefly introduce the disease and procedure if they have not been discussed, the inadequacy of

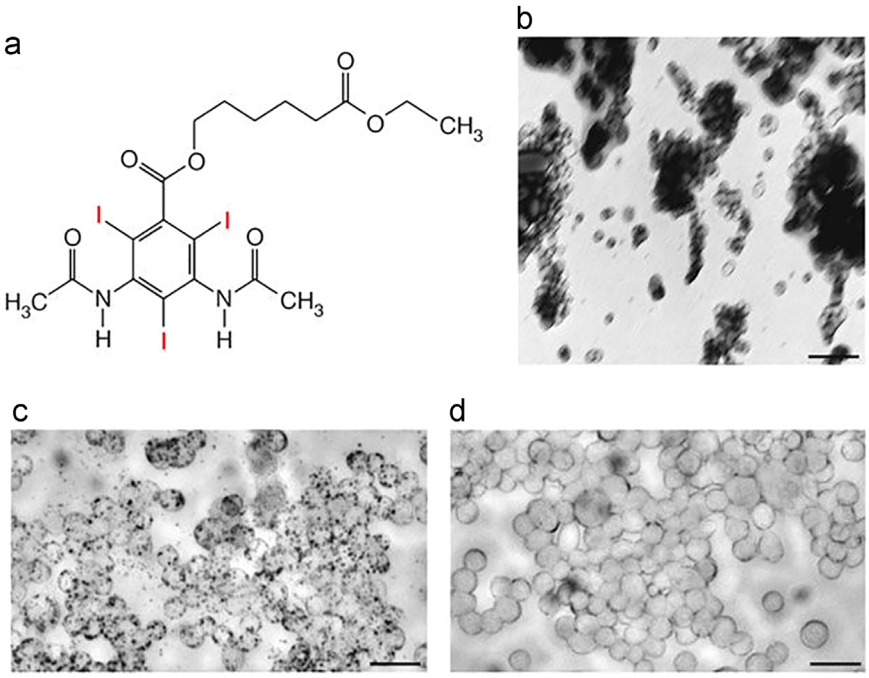

Figure 3 Properties of the contrast agent N1177. (a) Schematic representation of the iodinated compound of the contrast agent N1177 with the three iodine atoms in red. (b) Electron microscopic view of N1177 showing electron-dense iodinated granules coated by polymers appearing as negative prints after staining with a solution of uranyl acetate. Note the various sizes and shapes of nanoparticles found in the suspension. Scale bar, 100 nm. (c and d) Optical microscopy in a phase-contrast mode of macrophages after 1 h incubation *in vitro* with N1177 (c) or with the conventional CT contrast agent (d). Numerous dark granules were visualized only in the cytoplasm of macrophages incubated with N1177. Scale bar, 100 µm. (Reprinted from Fig. 1 in Ref. 61 with permission).

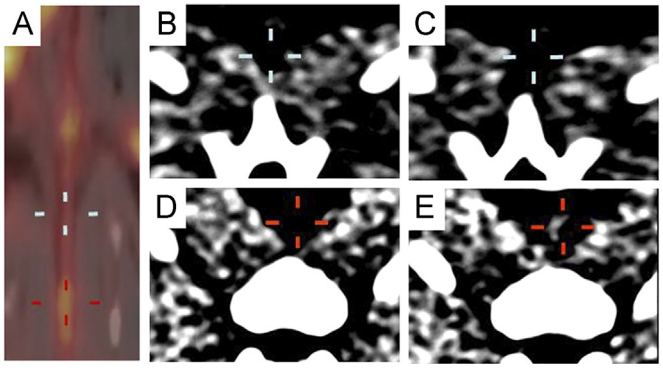

Figure 4 N1177-enhanced CT and corresponding ^{18}F-FDG PET of aorta from atherosclerotic rabbit. Fused PET/CT coronal view of aorta obtained at 3 h after injection of ^{18}F-FDG (A) and corresponding axial aortic sections acquired before (B and D) and at 2 h after injection of N1177 (C and E). In same rabbit, aortic regions with high (A; red cross) and low (A; blue cross) activities identified with PET at 3 h after injection of ^{18}F-FDG were associated with strong (E; red cross) and weak (C; blue cross) intensities of enhancement detected with CT at 2 h after injection of N1177 on corresponding axial views, respectively. (Reprinted from Fig. 2 in Ref. 63 with permission).

current devices and how radiopaque polymeric materials could improve these shortcomings.

One of the most used strategies in developing radiopaque polymer is to incorporate radiopaque materials in the polymer. Radiopaque materials include small molecular weight salts or compounds or nanoparticles containing iodine, barium, tantalum, bismuth, or gold. These radiopaque materials can be either blended into the polymer during the manufacturing at a specific ratio or infused into the manufactured polymer by organic solvent treatment.

3.2.1. *Embolic and chemoembolic materials*

Chemoembolization is an effective intervention for liver tumor treatment. In a typical procedure, a viscous drug carrier (the embolic agent) is mixed with contrast agent and injected through the portal vein under X-ray guidance for optimal embolization result. A variety of radiopacifiers, such as barium sulphate[67] and silver iodide complexes[68], were also used to introduce radiopacity. Barium sulfate-containing alginate microspheres[69], tantalum-containing polyurethane microspheres[70] and various zinc-silicate bioglasses[71,72] were also tested. Among all these studies, the most

common and incorporated radiopaque agent is still organoiodine compound.

Reports of the research and development of radiopaque embolization beads using organoiodine compounds appeared as early as the 1980s[73–78]. Poly(2-hydroxyethymethacrylate) was among the first hydrogels used in the research. Iodine based contrast agent was covalently linked with the hydrogel *via* acylation with 3-acetylamino-2,4,6-triiodobenzoyl chloride to introduce radiopacity. Alternatively, radiopacity could also be introduced *via* radical polymerization using 2-[4-iodobenzoyloxy]-ethyl methacrylate[79]. Surface functionalization could also be achieved by binding new monomer. For example, acrylic microspheres were synthesized from methyl methacrylate, methacrylic acid and 2-[4-iodobenzoyloxy]-ethyl methacrylate[80]. Methacrylic acid served as a carboxylic acid group source on the microsphere surface for thrombin immobilization. The microspheres were visible under X-ray when inserted into a rabbit cadaver, and the radiopacity was dependent on iodine concentration. The conjugated thrombin on the surface captured fibrin, accelerated sphere aggregation, and induced additional thrombin generation *in vitro*.

Another commonly used material is polyvinyl alcohol. Radiopacity can be introduced by covalent linkage of organoiodine compounds[81,82], insertion of Lipiodol into the microsphere[83], coacervation of Lipiodol with polyvinyl alcohol at the cloud point of the polyvinyl alcohol solution followed by cross-linking reaction[84], or multiple emulsions followed by cross-linking reaction[85]. Biocompatibles Inc. produced polyvinyl alcohol based beads, and they have been studied in the development of radiopaque drug eluting beads[86–88]. Radiopacity was introduced by loading Lipiodol into the polyvinyl alcohol hydrogel microspheres (100–300 μm)[83]. The iodine content by weight in the radiopaque microspheres reached 35.7%, and the loading was high enough to produce visible CT attenuation *in vivo*. Then doxorubicin was loaded into the radiopaque beads to create radiopaque drug eluding beads (Fig. 5)[89]. The impact of bead size to local drug distribution following transcatheter arterial chemoembolization was also studied[90]. Small beads (70–150 μm) and large beads (100–300 μm) were prepared from loading DC/LC Beads with doxorubicin and Lipiodol and injected into normal swine liver and kidney. It was observed that small beads penetrated farther into the distal regions and created a higher spatial frequency and a more homogeneous distribution than large beads (Fig. 6)[90]. The distance of drug penetration from the bead surface into the tissue was similar between small and large beads. Thus, small beads resulted in a

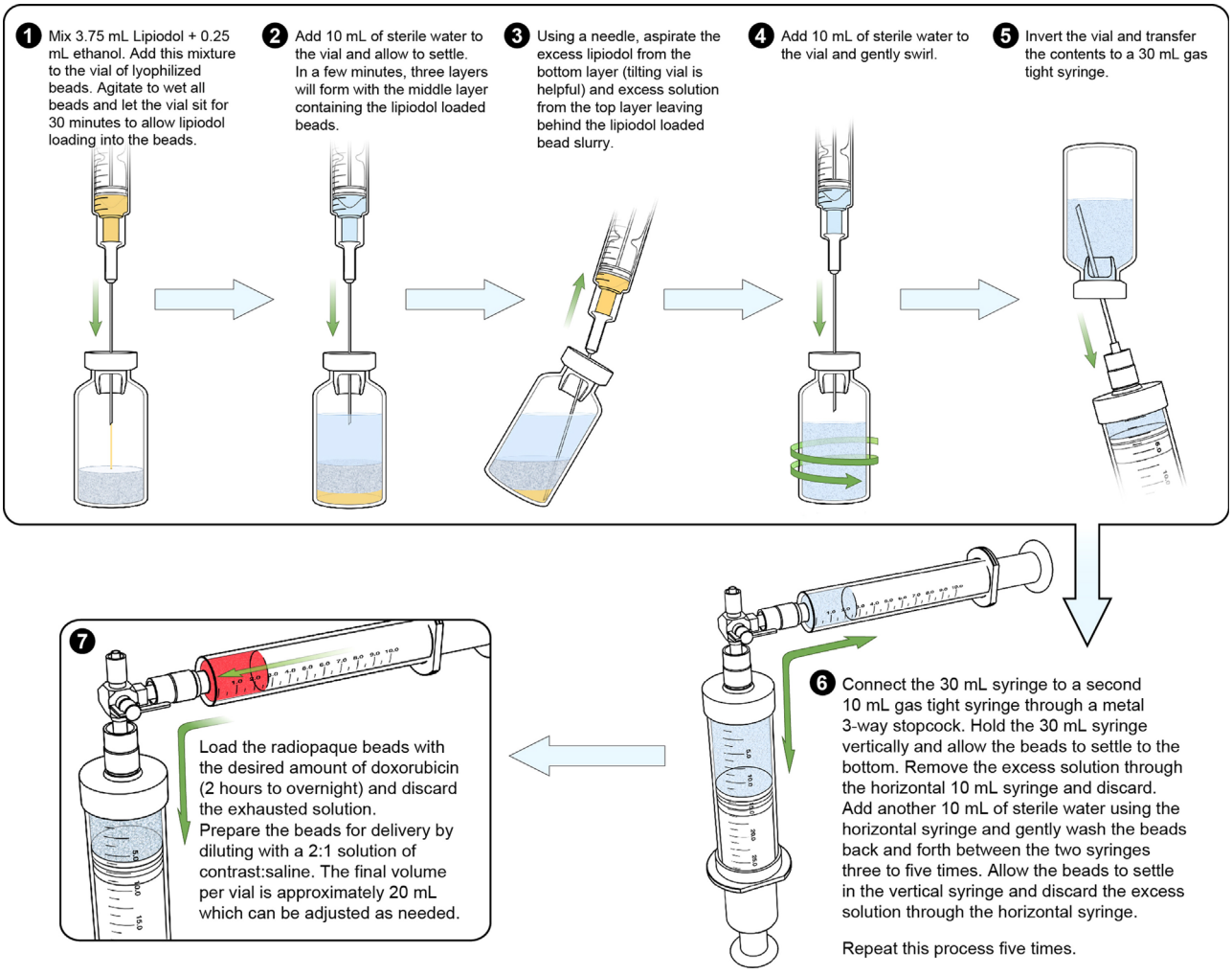

Figure 5 Summary of procedural steps for generating radiopaque drug eluting beads. (Reprinted from Ref. 89 with permission).

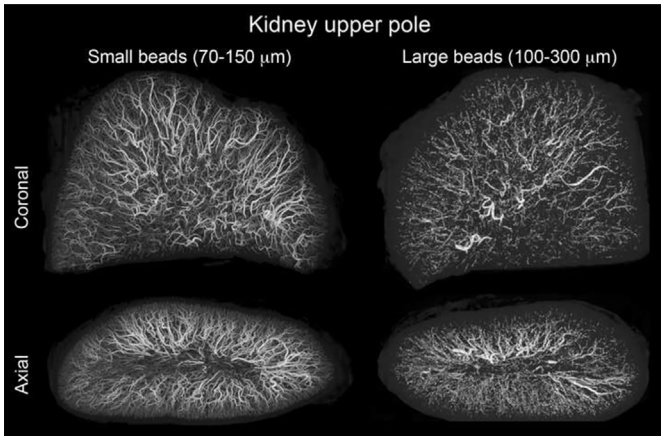

Figure 6 MicroCT of swine kidney tissue embolized with radiopaque drug eluting beads. Small (70–150 μm) and large (100–300 μm) beads are displayed with consistent size scaling. Small beads penetrate to more distal regions and yield a greater spatial density. (Reprinted from Fig. 2 in Ref. 90 with permission).

higher and more uniform drug coverage in the targeted tissues. When evaluated on a rabbit liver VX2 tumor model, the mean tumoral doxorubicin concentration in the group treated by the small beads almost tripled the group treated by the large beads, which was statistically significant. However, the plasma doxorubicin and doxorubicinol pharmacokinetics profiles were similar between the two groups[91].

Depending on the physical properties of the embolic agent, there are permanent and temporary embolizations. For liver chemoembolization, temporary embolization is desired due to the requirement of repetitive treatment. While permanent embolization has many choices of the embolic agent, temporary embolization essentially has only one commonly used agent, gelatin sponge. Gelatin is degraded by enzymes *in vivo* to achieve the temporary embolization. However, this degradation is unpredictable and unwanted early recanalization or permanent occlusion may occur. To better monitor not only the *in vivo* degradation but also the injection of the plugs, Venkatraman's group developed a radiopaque embolic plug based on synthetic polymers[92] The core of the plug consisted of poly(D,L-lactide-*co*-glycolide) (PLGA, molar ratio 50/50, MW = 90,000 g/mol). Different amounts of barium sulfate, tantalum, and bismuth (III) oxychloride were used as radiopaque fillers and co-extruded with PLGA. Bismuth and tantalum yielded brighter and sharper images, and the addition of all fillers lowered the glass transition temperature (T_g) of PLGA. To introduce the shape memory effect of the plug, T_g was further adjusted to slightly below the body temperature by mixing PEG (MW = 2000 g/mol) into the PLGA matrix. In the last step, crosslinked poly (ethylene glycol) diacrylate hydrogel was coated on the PLGA core to introduce water-responsive shape memory effect. *In vitro* degradation data suggested a 90% decrease in PLGA MW by day 25 but less than 50% mass loss by day 30. Then at day 70, the mass loss was 75%. *In vivo* evaluation on a rabbit model suggested the embolic plug was visible under fluoroscopy without the assistant of additional contrast agent. Embolic plug shape change and complete vascular occlusion was achieved within 2 min.

3.2.2. *Stent filler*

A strategy similar to the previous section is used on the research and development of radiopaque biodegradable polymeric stents. Radiopaque materials are usually blended with the polymer to introduce radiopacity, such as barium sulfate blended in PLA[93–95]. The resulting polymers have been applied to biliary and ureteral stents. For example, a biliary stent can be inserted into the bile duct in the treatment of bile leaks[93]. The biodegradable and radiopaque fiber was manufactured by first blending 96 L/4D PLA with 23% (*w*/*w*) $BaSO_4$ using melt spinning then solid-state drawing. Then the fiber was braided into a tubular mesh to create the stent. These biodegradable and radiopaque stents were observed to be intact at 3 months and degraded in 6 months, and they were as effective in the treatment of bile leaks as compared to the control polyethylene stents.

3.2.3. *Filler on intracranial aneurysm coils*

An intracranial aneurysm is a balloon developed on an intracranial vessel. If the aneurysm ruptures, a subarachnoid hemorrhage occurs, which over 25,000 people develop yearly. Treatment of intracranial aneurysms includes surgical clipping and embolization coiling. Embolization coiling achieved slightly better clinical outcomes than surgical clipping on patients with ruptured aneurysms[96]. Embolization coiling is an interventional procedure, where soft platinum coils are deployed through catheters to fill the aneurysm. Then natural clotting occurs around the coils and further blood flow is prevented into the aneurysm. However, the long term clinical outcome of embolization coiling showed an aneurysm recanalization rate up to 15%. One contributing factor to the recanalization is the inert surface of the platinum coils[97]. Such an inert surface discourages endothelial cell adhesion and an organized thrombus structure. When a thrombus is loosened, blood flow can reenter the aneurysm, and recanalization occurs. A stent may be placed at the neck of a wide neck aneurysm to assist the embolization coiling[98]. Alternatively, the coil surface can been modified with bioactive materials, such as collagen or shape memory polymers to improve clotting and scarring, stabilize thrombus and speed up aneurysm occlusion. Total polymeric coils have also been developed for these purposes.

In order to address the aforementioned issues, Hampikian et al. developed a radiopaque total polymeric coil[99]. In this coil, a shape memory polymer Calomer™ was investigated as the coil candidate. Tantalum metal powder (325 mesh) was used as the radiopaque filler at a volume fraction of 3% and weight fraction

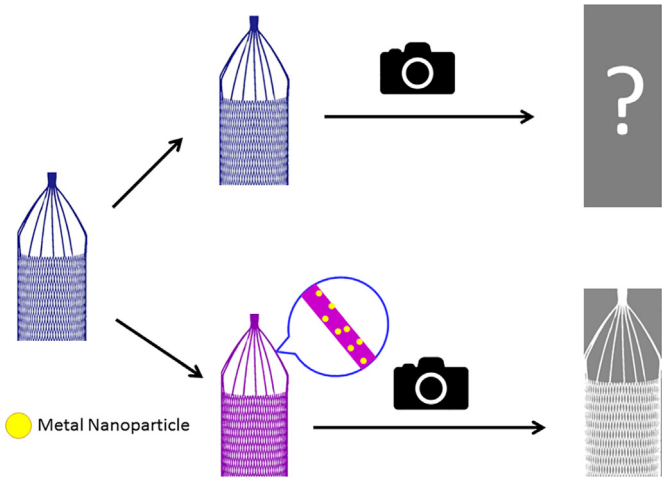

Figure 7 Illustration of the generation of radiopaque PPDO IVCF by gold nanoparticle (AuNP) infusion.

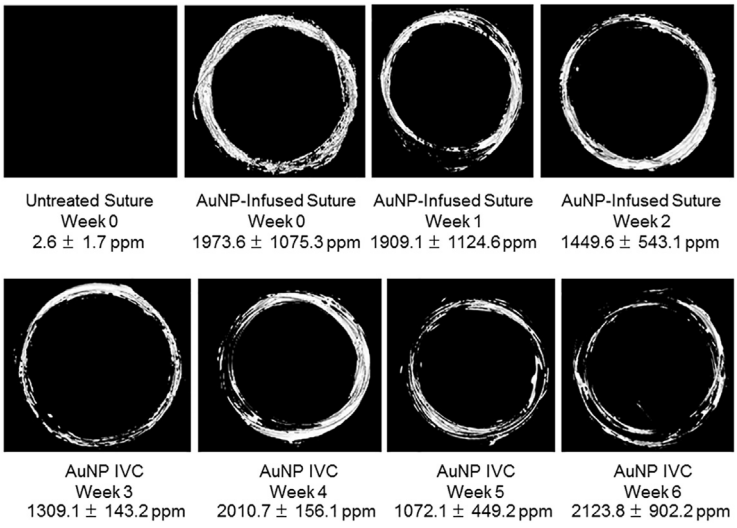

Figure 8 Long-term exposure to physiologic conditions did not affect radiopacity or gold content of gold nanoparticle–infused PPDO sutures. AuNP-infused PPDO sutures were suspended in PBS at 37 °C for up to 10 weeks. Three sutures were collected each week and imaged by micro-CT to determine radiopacity. Representative images over weeks 1–6 of the observation period are shown. The gold content was measured by ICP-OES, and the numeric result in ppm is listed under each image. All AuNP-infused PPDO sutures maintained radiopacity, and gold content did not decrease significantly during weeks 0–6 (one-way ANOVA, $p = 0.778$). (Reprinted from Fig. 7 in Ref. 101 with permission).

of 50%. The addition of tantalum powder introduced a small decrease in T_g and shape recovery force but did not affect the shape recovery process or the *in vitro* deployment. The radiopacity of the coils was confirmed by clinical X-ray imaging.

3.2.4. *Radiopaque infera vena cava filters*

Our group recently engaged in the development of radiopaque and resorbable infera vena cava filters (IVCFs)[100,101]. IVCFs are indicated for at-risk patients who are contraindicated with anticoagulants. The filters are deployed to inferior vena cava to capture thrombi and prevent them from traveling to the organs and cause fatal stoppage of blood flow. There are two types of IVCFs—permanent and temporary. Temporary IVCFs are meant to be removed after 5–6 weeks when the patients are no longer at risk. Failure of removal may cause fatal and costly complications. However, around half of the patients do not return to receive the surgical removal[102]. Thus, a resorbable IVCF based on polydioxanone (PPDO) is developed. However, PPDO is radiolucent and PPDO IVCFs cannot be easily monitored during the deployment or for long term stability. Therefore, our group developed radiopaque PPDO materials for use as ICVF (Fig. 7). PPDO expands but does not dissolve in some organic solvents, such as dichloromethane or chloroform. At the same time, certain organoiodine contrast agents and hydrophobic metal nanoparticles dissolve in dichloromethane or chloroform. Thus, we infused PPDO with organoiodine compounds, and the resulting PPDO had significant enhanced radiopacity on both X-ray and micro-CT and maintained the mechanical strength and biocompatibility compared to untreated PPDO[100]. We further improved the contrast agent by using 2- and 4-nm hydrophobic gold nanoparticles. Due to the higher Z number of gold, the radiopacity was even stronger than iodine infused PPDO, and the gold content and radiopacity remained stable over 6 weeks, which is the expected dwell time of the temporary ICVF[101] (Fig. 8).

4. Conclusions

Many studies have been focused on the improvement of diagnostic imaging and the visualization of catheterization related agents and devices, and aim at decreasing toxicity of current contrast agents, increasing visibility of specific targets in the vascular diseases to achieve a better diagnosis, and more importantly, a better visibility of the agents and devices. The usage of polymer-based agents and devices can achieve decreased toxicity, better biocompatibility, and a more controlled degradability when compared to small molecular contrast agents and metal based devices. However, most polymers are radiolucent and invisible on conventional imaging modalities, such as X-ray and CT. The development of radiopaque nanoparticle- and polymer-based embolic agents and devices could increase specificity of diagnostic imaging and monitoring of catheterization procedures and their outcomes.

Acknowledgments

This work was supported in part by grants from the American Heart Association (No. 15BGIA25690005), The University of Texas MD Anderson Cancer Center (Institutional Research Grant), and the National Institutes of Health (No. 1R56HL131633-01).

References

1. National Heart, Lung, Blood Institute. NHLBI fact book, fiscal year 2012. February 2013 [Cited 2016 Aug 7]. Available from: ⟨https://www.nhlbi.nih.gov/files/docs/factbook/FactBook2012.pdf⟩.
2. Mozaffarian D, Benjamin EJ, Go AS, Arnett DK, Blaha MJ, Cushman M, et al. Heart disease and stroke statistics—2016 update: a report from the american heart association. *Circulation* 2016;**133**:e38–360.
3. Laslett LJ, Alagona P, Clark III BA, Drozda Jr JP, Saldivar F, Wilson SR, et al. The worldwide environment of cardiovascular disease: prevalence, diagnosis, therapy, and policy issues: a report from the American College of Cardiology. *J Am Coll Cardiol* 2012;**60**:S1–49.
4. Benjamin EJ, Blaha MJ, Chiuve SE, Cushman M, Das SR, Deo R, et al. Heart disease and stroke statistics—2017 update: a report from the American Heart Association. *Circulation* 2017;**135**:e146–603.
5. Garcìa-Garcìa HM, Gogas BD, Serruys PW, Bruining N. IVUS-based imaging modalities for tissue characterization: similarities and differences. *Int J Cardiovasc Imaging* 2011;**27**:215–24.
6. Nissan SE, Yuck P. Intravascular ultrasound: novel pathophysiological insights and current clinical applications. *Circulation* 2001;**103**:604–11.
7. Saeed M, Hetts SW, English J, Wilson M. MR fluoroscopy in vascular and cardiac interventions. *Int J Cardiovasc Imaging* 2012;**28**:117–37.
8. Athanasoulis CA. Vascular radiology: looking into the past to learn about the future. *Radiology* 2001;**218**:317–22.
9. Raff GL, Gallagher MJ, O'Neill WW, Goldstein JA. Diagnostic accuracy of noninvasive coronary angiography using 64-slice spiral computed tomography. *J Am Coll Cardiol* 2005;**46**:552–7.
10. Budoff MJ, Shinbane JS. *Cardiac CT imaging: diagnosis of cardiovascular disease*. London: Springer; 2016.
11. Lamel DA. *The correlated lecture laboratory series in diagnostic radiological physics*. San Francisco: U.S. Deptment of Health and Human Services; 1981.
12. Saldana-Gonzalez G, Reyes U, Salazar H, Martínez O, Moreno E, Conde R. High density devices applied to a gamma-camera implementation. In: Ventzas D, editor. *Advanced Image Acquisition, Processing Techniques and Applications*. Rijeka, Croatia: INTECH; 2012.
13. Chhour P, Cheheltani R, Naha PC, Litt HI, Ferrari VA, Cormode DP. Nanoparticles for Cardiovascular Imaging with CT. In: Bulte JW, Modo MM, editors. *Design and Applications of Nanoparticles in Biomedical Imaging*. Cham: Springer; 2017. p. 357–84.
14. Lusic H, Grinstaff MW. X-ray-computed tomography contrast agents. *Chem Rev* 2012;**113**:1641–66.
15. Galper MW, Saung MT, Fuster V, Roessl E, Thran A, Proksa R, et al. Effect of computed tomography scanning parameters on gold nanoparticle and iodine contrast. *Invest Radiol* 2012;**47**:475–81.
16. Bourin M, Jolliet P, Ballereau F. An overview of the clinical pharmacokinetics of X-ray contrast media. *Clin Pharmacokinet* 1997;**32**:180–93.
17. Goldenberg I, Matetzky S. Nephropathy induced by contrast media: pathogenesis, risk factors and preventive strategies. *CMAJ* 2005;**172**:1461–71.
18. Pasternak JJ, Williamson EE. Clinical pharmacology, uses, and adverse reactions of iodinated contrast agents: a primer for the non-radiologist. *Mayo Clin Proc* 2012;**87**:390–402.
19. Aspelin P. Why choice of contrast medium matters. *Eur Radiol Suppl* 2006;**16**:D22–7.
20. Christiansen C. X-ray contrast media—an overview. *Toxicology* 2005;**209**:185–7.
21. McClennan BL, Preston M. Hickey memorial lecture. Ionic and nonionic iodinated contrast media: evolution and strategies for use. *AJR Am J Roentgenol* 1990;**155**:225–33.
22. Coche EE, Hammer FD, Goffette PP. Demonstration of pulmonary embolism with gadolinium-enhanced spiral CT. *Eur Radiol* 2001;**11**:2306–9.
23. Schmitt-Willich H, Brehm M, Ewers CL, Michl G, Müller-Fahrnow A, Petrov O, et al. Synthesis and physicochemical characterization of a new gadolinium chelate: the liver-specific magnetic resonance imaging contrast agent Gd-EOB-DTPA. *Inorg Chem* 1999;**38**:1134–44.
24. Bruneton JN, Falewée MN, François E, Cambon P, Philip C, Riess JG, et al. Liver, spleen, and vessels: preliminary clinical results of CT with perfluorooctylbromide. *Radiology* 1989;**170**:179–83.
25. Oliva MR, Erturk SM, Ichikawa T, Rocha T, Ros PR, Silverman SG, et al. Gastrointestinal tract wall visualization and distention during abdominal and pelvic multidetector CT with a neutral barium sulphate suspension: comparison with positive barium sulphate suspension and with water. *JBR-BTR* 2012;**95**:237–42.
26. Mette D, Strunk R, Zuccarello M. Cerebral blood flow measurement in neurosurgery. *Transl Stroke Res* 2011;**2**:152–8.
27. Carlson AP, Brown AM, Zager E, Uchino K, Marks MP, Robertson C, et al. Xenon-enhanced cerebral blood flow at 28% xenon provides uniquely safe access to quantitative, clinically useful cerebral blood flow information: a multicenter study. *Am J Neuroradiol* 2011;**32**:1315–20.
28. Thiriet M, Delfour M, Garon A. Vascular stenosis: an introduction: hemodynamics and drug elution. In: Lanzer P, editor. *PanVascular Medicine*. Berlin Heidelberg: Springer; 2015. p. 781–868.
29. Kang WC, Park CH, Chung WJ, Han SH, Ahn TH, Shin EK. Severe pulmonary artery stenosis caused by extrinsic compression of a calcified circular ring. *Circulation* 2005;**112**:e76–8.
30. Feig JE, Feig JL, Kini AS. Statins, atherosclerosis regression and HDL: insights from within the plaque. *Int J Cardiol* 2015;**189**:168–71.
31. Bentzon JF, Otsuka F, Virmani R, Falk E. Mechanisms of plaque formation and rupture. *Circ Res* 2014;**114**:1852–66.
32. Yusuf S, Hawken S, Ôunpuu S, Dans T, Avezum A, Lanas F, et al. Effect of potentially modifiable risk factors associated with myocardial infarction in 52 countries (the INTERHEART study): case-control study. *Lancet* 2004;**364**:937–52.
33. Lim SS, Vos T, Flaxman AD, Danaei G, Shibuya K, Adair-Rohani H, et al. A comparative risk assessment of burden of disease and injury attributable to 67 risk factors and risk factor clusters in 21 regions, 1990–2010: a systematic analysis for the Global Burden of Disease Study 2010. *Lancet* 2013;**380**:2224–60.

34. Ross R. Atherosclerosis—an inflammatory disease. *N Engl J Med* 1999;**340**:115–26.
35. Ornish D, Brown SE, Billings JH, Scherwitz LW, Armstrong WT, Ports TA, et al. Can lifestyle changes reverse coronary heart disease?: the lifestyle heart trial. *Lancet* 1990;**336**:129–33.
36. Hunninghake DB. HMG CoA reductase inhibitors. *Curr Opin Lipidol* 1992;**3**:22–8.
37. Weber C, Soehnlein O. *Atherosclerosis: treatment and prevention*. Boca Raton, FL: CRC Press; 2012.
38. Reape TJ, Groot PH. Chemokines and atherosclerosis. *Atherosclerosis* 1999;**147**:213–25.
39. Zernecke A, Shagdarsuren E, Weber C. Chemokines in atherosclerosis: an update. *Arterioscler Thromb Vasc Biol* 2008;**28**:1897–908.
40. Koenen RR, Weber C. Therapeutic targeting of chemokine interactions in atherosclerosis. *Nat Rev Drug Discov* 2010;**9**:141–53.
41. Van der Vorst EP, Döring Y, Weber C. Chemokines and their receptors in atherosclerosis. *J Mol Med* 2015;**93**:963–71.
42. Jones KL, Maguire JJ, Davenport AP. Chemokine receptor CCR5: from AIDS to atherosclerosis. *Br J Pharmacol* 2011;**162**:1453–69.
43. Noels H, Bernhagen J, Weber C. Macrophage migration inhibitory factor: a noncanonical chemokine important in atherosclerosis. *Trends Cardiovasc Med* 2009;**19**:76–86.
44. Burger-Kentischer A, Goebel H, Seiler R, Fraedrich G, Schaefer HE, Dimmeler S, et al. Expression of macrophage migration inhibitory factor in different stages of human atherosclerosis. *Circulation* 2002;**105**:1561–6.
45. Huo Y, Ley KF. Role of platelets in the development of atherosclerosis. *Trends Cardiovasc Med* 2004;**14**:18–22.
46. Arazi HC, Badimon JJ. Anti-inflammatory effects of anti-platelet treatment in atherosclerosis. *Curr Pharm Des* 2012;**18**:4311–25.
47. Von Hundelshausen P, Schmitt MM. Platelets and their chemokines in atherosclerosis—clinical applications. *Front Physiol* 2014;**5**:294.
48. Lievens D, Von Hundelshausen P. Platelets in atherosclerosis. *Thromb Haemost* 2011;**106**:827–38.
49. Buffolo E, De Andrade JC, Branco JN, Teles CA, Aguiar LF, Gomes WJ. Coronary artery bypass grafting without cardiopulmonary bypass. *Ann Thorac Surg* 1996;**61**:63–6.
50. North American Symptomatic Carotid Endarterectomy Trial Collaborators, Barnett HJ, Taylor DW, Haynes RB, Sackett DL, Peerless SJ, et al. Beneficial effect of carotid endarterectomy in symptomatic patients with high-grade carotid stenosis. *N Engl J Med* 1991;**325**:445–53.
51. Torpy JM, Lynm C, Glass RM. Percutaneous coronary intervention. *JAMA* 2004;**291**:778.
52. Rosenbluth PR, Grossman R, Arias B. Accurate placement of artificial emboli: a problem in the treatment of cerebral angiomas by the embolization method. *JAMA* 1960;**174**:308–9.
53. Lopera JE. Embolization in trauma: principles and techniques. *Semin Interv Radiol* 2010;**27**:14–28.
54. Kato T, Nemoto R, Mori H, Takahashi M, Tamakawa Y. Transcatheter arterial chemoembolization of renal cell carcinoma with microencapsulated mitomycin C. *J Urol* 1981;**125**:19–24.
55. Chuang VP, Wallace S. Chemoembolization: transcatheter management of neoplasms. *JAMA* 1981;**245**:1151–2.
56. Guan YS, He Q, Wang MQ. Transcatheter arterial chemoembolization: history for more than 30 years. *ISRN Gastroenterol* 2012;**2012**:480650.
57. Kudo M. The 2008 Okuda lecture: management of hepatocellular carcinoma: from surveillance to molecular targeted therapy. *J Gastroenterol Hepatol* 2010;**25**:439–52.
58. Bhattacharya S, Novell JR, Winslet MC, Hobbs KE. Iodized oil in the treatment of hepatocellular carcinoma. *Br J Surg* 1994;**81**:1563–71.
59. Solans C, Izquierdo P, Nolla J, Azemar N, Garcia-Celma MJ. Nano-emulsions. *Curr Opin Colloid Interface Sci* 2005;**10**:102–10.
60. Robbins CS, Hilgendorf I, Weber GF, Theurl I, Iwamoto Y, Figueiredo JL, et al. Local proliferation dominates lesional macrophage accumulation in atherosclerosis. *Nat Med* 2013;**19**:1166–72.
61. Hyafil F, Cornily JC, Feig JE, Gordon R, Vucic E, Amirbekian V, et al. Noninvasive detection of macrophages using a nanoparticulate contrast agent for computed tomography. *Nat Med* 2007;**13**:636–41.
62. Van Herck JL, De Meyer GR, Martinet W, Salgado RA, Shivalkar B, De Mondt R, et al. Multi-slice computed tomography with N1177 identifies ruptured atherosclerotic plaques in rabbits. *Basic Res Cardiol* 2010;**105**:51.
63. Hyafil F, Cornily JC, Rudd JH, Machac J, Feldman LJ, Fayad ZA. Quantification of inflammation within rabbit atherosclerotic plaques using the macrophage-specific CT contrast agent N1177: a comparison with ^{18}F-FDG PET/CT and histology. *J Nucl Med* 2009;**50**:959–65.
64. Cormode DP, Roessl E, Thran A, Skajaa T, Gordon RE, Schlomka JP, et al. Atherosclerotic plaque composition: analysis with multicolor CT and targeted gold nanoparticles. *Radiology* 2010;**256**:774–82.
65. Constantinides P. Plaque fissures in human coronary thrombosis. *J Atheroscler Res* 1966;**6**:1–17.
66. Winter PM, Shukla HP, Caruthers SD, Scott MJ, Fuhrhop RW, Robertson JD, et al. Molecular imaging of human thrombus with computed tomography. *Acad Radiol* 2005;**12**:S9–13.
67. Thanoo BC, Sunny MC, Jayakrishnan A. Preparation and properties of barium sulphate and methyl iothalamate loaded poly(vinyl alcohol) microspheres as radiopaque particulate emboli. *J Appl Biomater* 1991;**2**:67–72.
68. Horák D, Červinka M, Půža V. Radiopaque poly(2-hydroxyethyl methacrylate) particles containing silver iodide complexes tested on cell culture. *Biomaterials* 1998;**19**:1303–7.
69. Wang Q, Qian K, Liu S, Yang Y, Liang B, Zheng C, et al. X-ray visible and uniform alginate microspheres loaded with *in situ* synthesized $BaSO_4$ nanoparticles for *in vivo* transcatheter arterial embolization. *Biomacromolecules* 2015;**16**:1240–6.
70. Thanoo BC, Sunny MC, Jayakrisnnan A. Tantalum-loaded polyurethane microspheres for particulate embolization: preparation and properties. *Biomaterials* 1991;**12**:525–8.
71. Kehoe S, Langman M, Werner-Zwanziger U, Abraham RJ, Boyd D. Mixture designs to assess composition–structure–property relationships in SiO_2–CaO–ZnO–$La2O_3$–TiO_2–MgO–SrO–Na_2O glasses: potential materials for embolization. *J Biomater Appl* 2013;**28**:416–33.
72. Hasan M, Kehoe S, Boyd D. Temporal analysis of dissolution by-products and genotoxic potential of spherical zinc–silicate bioglass: "imageable beads" for transarterial embolization. *J Biomater Appl* 2014;**29**:566–81.
73. Horák D, Švec F, Kálal J, Gumargalieva K, Adamyan A, Skuba N, et al. Hydrogels in endovascular embolization. I. Spherical particles of poly(2-hydroxyethyl methacrylate) and their medico-biological properties. *Biomaterials* 1986;**7**:188–92.
74. Horák D, Šeksvec F, Kálal J, Adamyan AA, Volynskii YD, Voronkova OS, et al. Hydrogels in endovascular embolization. II. Clinical use of spherical particles. *Biomaterials* 1986;**7**:467–70.
75. Horák D, Metalová M, Švec F, Drobník J, Kálal J, Borovička M, et al. Hydrogels in endovascular embolization. III. Radiopaque spherical particles, their preparation and properties. *Biomaterials* 1987;**8**:142–5.
76. Horák D, Švec F, Kálal J, Adamyan A, Skuba N, Titova M, et al. Hydrogels in endovascular embolization: IV. Effect of radiopaque spherical particles on the living tissue. *Biomaterials* 1988;**9**:367–71.
77. Horák D, Švec F, Adamyan A, Titova M, Skuba N, Voronkova O, et al. Hydrogels in endovascular embolization: V. Antitumour agent methotrexate-containing p[HEMA]. *Biomaterials* 1992;**13**:361–6.
78. Horák D, Červinka M, Půža V. Hydrogels in endovascular embolization: VI. Toxicity tests of poly(2-hydroxyethyl methacrylate) particles on cell cultures. *Biomaterials* 1997;**18**:1355–9.
79. van Hooy-Corstjens CS, Saralidze K, Knetsch ML, Emans PJ, de Haan MW, Magusin PC, et al. New intrinsically radiopaque hydrophilic microspheres for embolization: synthesis and characterization. *Biomacromolecules* 2008;**9**:84–90.

80. Saralidze K, van Hooy-Corstjens CS, Koole LH, Knetsch ML. New acrylic microspheres for arterial embolization: combining radiopacity for precise localization with immobilized thrombin to trigger local blood coagulation. *Biomaterials* 2007;**28**:2457–64.
81. Negussie AH, Dreher MR, Johnson CG, Tang Y, Lewis AL, Storm G, et al. Synthesis and characterization of image-able polyvinyl alcohol microspheres for image-guided chemoembolization. *J Mater Sci Mater Med* 2015;**26**:198.
82. Duran R, Sharma K, Dreher MR, Ashrafi K, Mirpour S, Lin M, et al. A novel inherently radiopaque bead for transarterial embolization to treat liver cancer—a Pre-clinical study. *Theranostics* 2016;**6**:28–39.
83. Sharma KV, Dreher MR, Tang Y, Pritchard W, Chiesa OA, Karanian J, et al. Development of "imageable" beads for transcatheter embolotherapy. *J Vasc Interv Radiol* 2010;**21**:865–76.
84. Lu XJ, Zhang Y, Cui DC, Meng WJ, Du LR, Guan HT, et al. Research of novel biocompatible radiopaque microcapsules for arterial embolization. *Int J Pharm* 2013;**452**:211–9.
85. Meng WJ, Lu XJ, Wang H, Fan TY, Cui DC, Zhang SS, et al. Preparation and evaluation of biocompatible long-term radiopaque microspheres based on polyvinyl alcohol and lipiodol for embolization. *J Biomater Appl* 2015;**30**:133–46.
86. Ashrafi K, Tang Y, Britton H, Domenge O, Blino D, Bushby AJ, et al. Characterization of a novel intrinsically radiopaque drug-eluting bead for image-guided therapy: DC Bead LUMI™. *J Control Release* 2017;**250**:36–47.
87. Sharma KV, Bascal Z, Kilpatrick H, Ashrafi K, Willis SL, Dreher MR, et al. Long-term biocompatibility, imaging appearance and tissue effects associated with delivery of a novel radiopaque embolization bead for image-guided therapy. *Biomaterials* 2016;**103**:293–304.
88. Lewis AL, Dreher MR. Locoregional drug delivery using image-guided intra-arterial drug eluting bead therapy. *J Control Release* 2012;**161**:338–50.
89. Johnson CG, Tang Y, Beck A, Dreher MR, Woods DL, Negussie AH, et al. Preparation of radiopaque drug-eluting beads for transcatheter chemoembolization. *J Vasc Interv Radiol* 2016;**27**:117–26.e3.
90. Dreher MR, Sharma KV, Woods DL, Reddy G, Tang Y, Pritchard WF, et al. Radiopaque drug-eluting beads for transcatheter embolotherapy: experimental study of drug penetration and coverage in swine. *J Vasc Interv Radiol* 2012:257–64.e4.
91. Gholamrezanezhad A, Mirpour S, Geschwind JF, Rao P, Loffroy R, Pellerin O, et al. Evaluation of 70–150-μm doxorubicin-eluting beads for transcatheter arterial chemoembolization in the rabbit liver VX2 tumour model. *Eur Radiol* 2016;**26**:3474–82.
92. Wong YS, Salvekar AV, Zhuang KD, Liu H, Birch WR, Tay KH, et al. Bioabsorbable radiopaque water-responsive shape memory embolization plug for temporary vascular occlusion. *Biomaterials* 2016;**102**:98–106.
93. Laukkarinen J, Nordback I, Mikkonen J, Kärkkäinen P, Sand J. A novel biodegradable biliary stent in the endoscopic treatment of cystic-duct leakage after cholecystectomy. *Gastrointest Endosc* 2007;**65**:1063–8.
94. Lämsä T, Jin H, Mikkonen J, Laukkarinen J, Sand J, Nordback I. Biocompatibility of a new bioabsorbable radiopaque stent material ($BaSO_4$ containing poly-L,D-lactide) in the rat pancreas. *Pancreatology* 2006;**6**:301–5.
95. Nuutinen JP, Clerc C, Törmälä P. Mechanical properties and *in vitro* degradation of self-reinforced radiopaque bioresorbable polylactide fibres. *J Biomater Sci Polym Ed* 2003;**14**:665–76.
96. Li J, Su L, Ma J, Kang P, Ma L, Ma L. Endovascular coiling *versus* microsurgical clipping for patients with ruptured very small intracranial aneurysms: management strategies and clinical outcomes of 162 cases. *World Neurosurg* 2017;**99**:763–9.
97. Piotin M, Mandai S, Murphy KJ, Sugiu K, Gailloud P, Martin JB, et al. Dense packing of cerebral aneurysms: an *in vitro* study with detachable platinum coils. *Am J Neuroradiol* 2000;**21**:757–60.
98. Luo CB, Wei CJ, Chang FC, Teng MM, Lirng JF, Chang CY. Stent-assisted embolization of internal carotid artery aneurysms. *J Chin Med Assoc* 2003;**66**:460–6.
99. Hampikian JM, Heaton BC, Tong FC, Zhang Z, Wong CP. Mechanical and radiographic properties of a shape memory polymer composite for intracranial aneurysm coils. *Mater Sci Eng C* 2006;**26**:1373–9.
100. Singhana B, Chen A, Slattery P, Yazdi IK, Qiao Y, Tasciotti E, et al. Infusion of iodine-based contrast agents into poly(*p*-dioxanone) as a radiopaque resorbable IVC filter. *J Mater Sci Mater Med* 2015;**26**:124.
101. Tian L, Lee P, Singhana B, Chen A, Qiao Y, Lu L, et al. Radiopaque resorbable inferior vena cava filter infused with gold nanoparticles. *Sci Rep* 2017;**7**:2147.
102. Rogers FB, Shackford SR, Horst MA, Miller JA, Wu D, Bradburn E, et al. Determining venous thromboembolic risk assessment for patients with trauma: the trauma embolic scoring system. *J Trauma Acute Care Surg* 2012;**73**:511–5.